ELSEVIER

Surface Science 474 (2001) 81–97

SURFACE SCIENCE

www.elsevier.nl/locate/susc

Segregation and ordering at $Fe_{1-x}Al_x(1\,0\,0)$ surfaces – a model case for binary alloys

V. Blum [a,*], L. Hammer [a], W. Meier [a], K. Heinz [a], M. Schmid [b], E. Lundgren [b,1], P. Varga [b]

[a] *Lehrstuhl für Festkörperphysik, Universität Erlangen-Nürnberg, Staudtstrasse 7, D-91058 Erlangen, Germany*
[b] *Institut für Allgemeine Physik, Technische Universität Wien, Wiedner Hauptstraße 8–10, A-1040 Wien, Austria*

Received 28 September 2000; accepted for publication 22 November 2000

Abstract

The geometrical structure, chemical order and composition of (1 0 0) oriented surfaces of the binary alloy system $Fe_{1-x}Al_x$ were investigated in the Fe-rich regime ($x = 0.03$, 0.15, and 0.30) using quantitative low-energy electron diffraction. Low-energy He^+ ion scattering and scanning tunneling microscopy were additionally employed to characterize the $x = 0.15$ sample. The equilibrium structures developing with increasing bulk Al content can be consistently explained by the interplay between Al surface segregation and ordering processes which are controlled by atomic interactions similar to those in the bulk. These interactions divide the process of Al segregation to the very surface into two steps whereby Al atoms occupy sites of two different sublattices of $c(2 \times 2)$ periodicity with different probability. Whilst one sublattice is already completely filled at low bulk Al concentration, the other sublattice fills only gradually with increasing bulk Al content. The local order in deeper layers is consistent with the bulk phase diagram.

Keywords: Alloys; Aluminum; Iron; Low energy electron diffraction (LEED); Low energy ion scattering (LEIS); Scanning tunneling microscopy; Surface relaxation and reconstruction; Surface segregation

1. Introduction

Much attention has been paid to alloys formed between Fe and Al for two reasons. First, this class of materials gives rise to a number of useful technological applications [1]. For example, Fe–Al alloys with low Al content have long been used as soft magnetic materials. The two ordered phases Fe_3Al and FeAl are of interest as candidate materials for structural applications [2,3]: their higher tensile strength compared to other Fe-based alloys teams up with their relatively low density and improved corrosion resistance due to the formation of protective Al_2O_3 layers when exposed to oxygen [5–7]. Their practical application is, however, still hampered by their relatively high brittleness due to environmental embrittlement [4], weak grain boundaries and vacancy hardening [3].

* Corresponding author. Tel.: +49-9131-85-28406; fax: +49-9131-85-28400.
E-mail address: v.blum@fkp.physik.uni-erlangen.de (V. Blum).
[1] Present address: Department of Synchrotron Radiation Research, Institute of Physics, University of Lund, Box 118, S-22100 Lund, Sweden.

0039-6028/01/$ - see front matter
PII: S0039-6028(00)00987-0

In other words, important structural properties of these materials such as deformation, fracture [8,9] or grain-boundary diffusion [10,11] involve internal defects such as interfaces, or their formation. Naturally, such interest has also stimulated work on the properties of Fe–Al alloy surfaces (for a recent review, see Ref. [12]). The relative ease of obtaining information on surface order and chemistry may provide important general insights into interfacial properties that would be difficult to attain otherwise.

Second, and from a more fundamental point of view, the Fe–Al system forms an ideal playground to study short- and long-range order phenomena in binary alloys as a function of both temperature and chemical composition. The system belongs to the class of ordering alloys, characterized by a relatively large heat of formation (0.26 eV per unit cell in stoichiometric FeAl [13]). Its phase diagram [14], the Fe-rich part of which is schematically depicted in Fig. 1, shows that a body centered cubic (bcc) arrangement forms the underlying atomic lattice in the entire composition range between 0 and 50 at.% Al. Already for the A2 solid solution phase that forms below approximately 20 at.% Al, a clear tendency towards short-range ordering is observed [15,16], with both first and second nearest neighbor interactions showing a strong preference for a heterogeneous occupation of the corresponding lattice sites. These interactions find their expression in the formation of long-range $D0_3$ type order for slightly higher Al contents (20–35 at.% Al; ideal stoichiometry: Fe_3Al), and B2 type order (ideal stoichiometry:

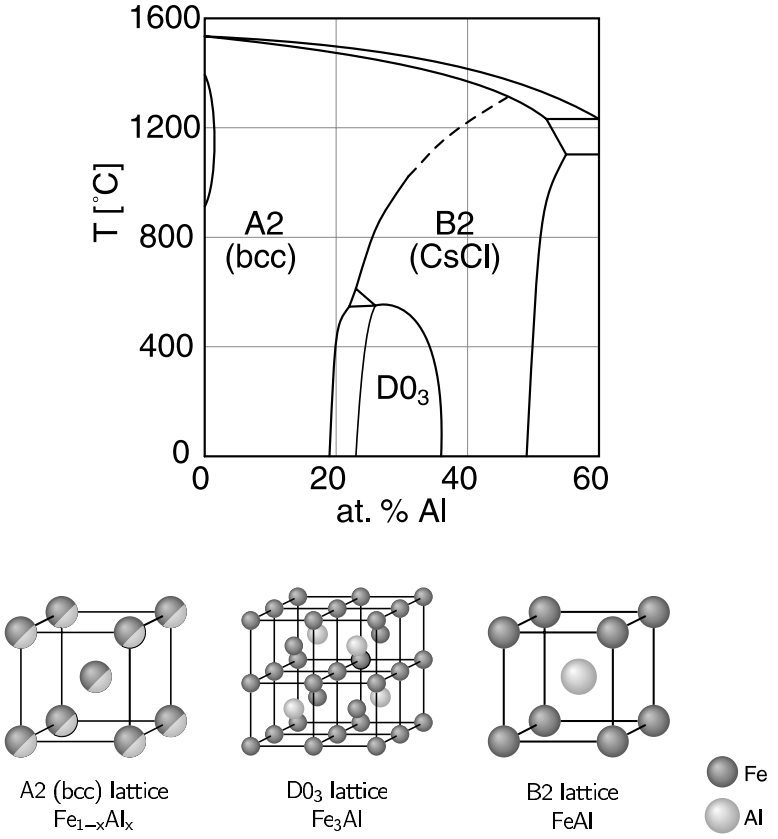

Fig. 1. Schematic reproduction of the Fe-rich part of the Fe–Al phase diagram after Ref. [14] (upper panel). The regions of the three structurally different phases A2, $D0_3$ and B2 are indicated. Their respective atomic structures are depicted in the lower panel. The remaining areas of the phase diagram include the "γ-loop" (fcc Fe) and regions of two-phase equilibria.

FeAl) for yet more Al. Finally, the system shows the two possible order–disorder transitions $D0_3 \leftrightarrow$ B2 and B2 $\leftrightarrow$ A2 with concentration-dependent transition temperatures. All three bulk lattice types are visualized in the lower panel of Fig. 1.

Taking the surface into account, an alloy may reduce its total energy through the enrichment of one of the components at the very boundary to the vacuum (segregation). However, ordering tendencies will hamper segregation for the simple reason that the latter favors the occupation of neighboring lattice sites by the same atomic species at the surface while ordering causes exactly the opposite. This interplay between ordering and segregation at alloy surfaces has been the subject of a recent review article [17]. In the Fe–Al system, previous studies suggest a clear segregation tendency of Al in the entire Fe-rich range, even for the near or completely stoichiometric B2 compound FeAl. Studies using Auger electron spectroscopy (AES) for (1 1 0), (1 1 1), (2 1 0) and (3 1 0) oriented surfaces [18,19] and quantitative (surface) X-ray diffraction (S)XRD for the (1 1 0) face [20] leave this conclusion beyond doubt. For the case of Fe_3Al-(1 1 0), a nearly pure Al top layer has been found [21], and for the A2 phase region Al segregation has been qualitatively established by AES measurements [22].

Quantitative low-energy electron diffraction (LEED) studies of the (1 0 0) oriented surface for the equiatomic alloy FeAl show the topmost layer to be composed entirely of Al. No significant deviation from bulk chemical order occurs since the bulk-like B2 stacking sequence is consistent with such a termination [23,24]. [2] However, Al segregation to the (1 0 0) oriented Fe–Al alloy surface takes place for samples with lower Al content. For the A2 solid solution at low Al concentration, Al segregation has been qualitatively confirmed using AES and LEED [25,26]. On the (1 0 0) surface, two different structures have been reported, i.e. a c(2 × 2) arrangement for very low Al content (1 wt.% Al), and a (1 × 1) termination for 15 at.% Al (in the present work (1 × 1) symmetry refers to the bulk terminated A2 structure). In both cases, a quantitative surface structure determination is lacking. For the $D0_3$ range, the termination appears to be by a nearly complete layer of Al as shown by a quantitative LEED study of the Al depleted surface phase of a sample with nominal FeAl composition in the bulk [27]. Yet, a detailed analysis of the (1 0 0) surface of a bulk $D0_3$ sample is still missing.

It is the main goal of the present work to elucidate the interplay of ordering forces and Al segregation at $Fe_{1-x}Al_x$(1 0 0) surfaces in detail. To that end, we provide quantitative crystallographic analyses for samples with $x = 0.03$, 0.15, and 0.30 in the bulk using quantitative LEED. AES is used as a qualitative tool to monitor the overall surface composition, and also to characterize the conditions under which "equilibrium" is attained [28]. For $Fe_{0.85}Al_{0.15}$, low energy He^+ ion scattering (LEIS) and chemically resolved scanning tunneling microscopy (STM) give additional precise information on the topmost layer composition. STM also allows for a direct view of the lateral surface short-range order. As will be shown, these techniques together are able to paint a clear picture of the structural properties of $Fe_{1-x}Al_x$(1 0 0) surfaces.

2. Experimental and computational details

The LEED measurements were performed in an ultrahigh vacuum (UHV) chamber (Erlangen laboratory, base pressure of 2×10^{-11} mbar) equipped with a three-grid backview LEED optics and a hemispherical energy analyzer for AES studies. The sample holder allowed for heating to above 1300 K by electron bombardment from the rear and fast cooling by contact to a liquid nitrogen reservoir. Temperatures were measured using a $WRe_{3\%}$–$WRe_{25\%}$ thermocouple attached to the sample. In addition, the chamber was equipped with a sputter gun in order to clean the surface prior to each investigation. LEED intensity vs. energy spectra, $I(E)$, were recorded using

[2] A previous LEED result [27] claiming that Al segregates to the *second* layer of a FeAl(1 0 0) surface, replacing about 20% of its Fe atoms, may also be explained by an enhanced thermal vibrational amplitude of the atoms located there (details will be given in Ref. [24]).

a fast, computer-controlled video LEED system described elsewhere [29,30]. The data were taken after the sample had been quenched to below 100 K (2 min quenching time). Normal incidence of the primary electron beam was adjusted by comparison of spectra of symmetry-equivalent beams. Eventually, symmetry-equivalent spectra were averaged in order to reduce the influence of some residual misalignment and possible inhomogeneities of the luminescent screen, and to improve the signal-to-noise ratio.

For the $Fe_{0.85}Al_{0.15}$(1 0 0), additional measurements were performed by STM and LEIS in a similar apparatus (Vienna laboratory) with a comparable base pressure. The sample was prepared in exactly the same way as for the LEED/AES investigations, using the AES peak-to-peak ratio of Al (68 eV) vs. Fe (47 eV) to control the surface preparation. The STM studies were performed with an Omicron Micro STM. LEIS data for the topmost atomic layer was obtained with a primary He^+ ion beam of 1 keV energy impinging on the surface. In order to avoid elastic scattering contributions from the second and deeper layers of the crystal, the [0 1 1] azimuth was chosen for the investigations, using a scattering angle of 90° and specular scattering conditions. In order to eliminate any possible influence of sputter damage, the Fe/Al elastic peak ratio as a function of measuring time was extrapolated back to the beginning of the measurements. Instead of an independent quantification of the top layer composition using reference standards, such values were obtained by calibrating the signals obtained from different surface preparations against one another. The STM result for the surface composition of one of them was then used to quantitatively determine the other (see Section 4.2).

Quantitative LEED intensity analyses were performed using the TensErLEED program package [31]. This applies the tensor LEED perturbation method [32,33] for the variation of structural and non-structural parameters including the layer dependent concentration and ordering of chemical species and the vibrational amplitudes of surface atoms [34–36]. The best fit in the multidimensional parameter space is found by an automated structural search procedure [37] guided by the Pendry *R*-factor [38]. Error limits for the various parameters were estimated by the variance of the *R*-factor [38] neglecting, however, correlations between different parameters.

Several reference structures had to be used in the course of the structural search in order to stay within the validity range of tensor LEED. As this method does not allow to vary the (lateral) lattice parameter a within the perturbation scheme, a was instead adjusted also by applying different reference calculations. In view of the coupling between the inner potential V_{0r} and a [39], the accurate energy dependence of V_{0r} as computed by Rundgren [40] was used. For a pure Fe crystal this yields

$$V_{0r}^{Fe}(E) = V_{00} + \max\left(-10.3, 0.39 - \frac{76.63}{\sqrt{(E/\mathrm{eV}) + 9.68}} \right) \mathrm{eV} \quad (1)$$

(with the value of V_{00} adjusted during the fit procedure as usual) which was deemed accurate enough to represent the situation for both the $Fe_{0.97}Al_{0.03}$ and $Fe_{0.85}Al_{0.15}$ samples. For $Fe_{0.70}Al_{0.30}$, the analogous expression for a stoichiometric and fully ordered FeAl bulk crystal (B2 structure) was used which looks very similar to that for Fe, so justifying their use for cases of intermediate Al content. For both $Fe_{0.97}Al_{0.03}$ and $Fe_{0.85}Al_{0.15}$, the imaginary part of the inner potential describing the electron attenuation by inelastic scattering was kept constant at $V_{0i} = 5$ eV throughout the analysis and subsequently verified by test calculations. In the case of $Fe_{0.70}Al_{0.30}$, the independent adjustment of V_{0i} lead to a best-fit value of 5.5 eV. The atomic scattering for energies up to 500 eV was described by up to 13 fully relativistic and spin-averaged phase shifts. Within the structural search they were corrected for thermal atomic vibrations and static positional disorder described by mean square displacements (MSD) from the ideal lattice positions. Different MSD were allowed for atoms in the bulk and in the topmost and second layer. Additionally, element specific vertical displacements were considered for lattice sites with a sufficiently high occupation by either species.

The simultaneous optimization of elemental concentrations and element-dependent vibrational amplitudes on the same lattice site by LEED is hampered by a clear correlation between both quantities. While, technically, it is still possible to obtain best-fit values for both types of parameters, their error limits become quite large when the coupling is taken into account. At the same time, the fit becomes vulnerable even to small systematic errors in the model. In order to avoid introducing any unnecessary uncertainties into the LEED analyses, we did not attempt to independently determine the chemical order and/or composition of lattice sites for which accurate results from LEIS and STM were available. In particular, this holds for the topmost atomic layers of $Fe_{0.97}Al_{0.03}(1\,0\,0)$ and $Fe_{0.85}Al_{0.15}(1\,0\,0)$, the stoichiometry of which was fixed at the STM/LEIS values even for the final refinement stage in the LEED analyses. However, we did perform extensive tests in order to ensure that LEED and STM/LEIS results did not contradict one another – for example, with the set of model parameters used below, the LEED best fit for the top layer stoichiometry of $Fe_{0.85}Al_{0.15}$-$(1\,0\,0)$ deviates by only 5 at.% from STM/LEIS. A more detailed paper on this point is in progress [24].

3. Qualitative surface characterization

The $Fe_{1-x}Al_x$ samples used in the present work were grown, oriented and cut at the Max-Planck-Institut für Eisenforschung in Düsseldorf, Germany. The $x = 0.15$ sample was already used in a previous investigation of that group [26]. Both $Fe_{0.70}Al_{0.30}$ and $Fe_{0.85}Al_{0.15}$ required only a few sputter/anneal cycles to remove initial contaminants, after which no further impurities could be detected by AES. For the $Fe_{0.97}Al_{0.03}$ crystal, it proved impossible to avoid the two main contaminants, C and S, permanently. However, both could initially be removed by prolonged sputtering and did not return to the surface for annealing temperatures below 1150 K so that a contamination-free surface (as judged by AES) could be prepared.

The structure and composition of binary alloy surfaces often show a marked dependence on details of the sample preparation. Since the present work aims to investigate the ordering of Fe–Al surfaces in compositional equilibrium with the bulk, it is important to ascertain that such an equilibrium state has indeed been reached. In our case, the preparation procedure leads to an initial depletion of the entire surface *region* of Al through preferential sputtering. Compositional equilibrium between the bulk and the surface is then re-established by annealing the crystal at a sufficiently high temperature. The kinetics of this equilibration process has been described before [12,18,22,26,28], and the conditions at which compositional equilibrium is eventually attained for the present samples are discussed in detail in a separate publication [28].

Both the level of surface segregation and the degree of near-surface order to be discussed below are temperature-dependent phenomena. As described in Ref. [28], the surface structures presented below contain contributions from three different regimes of (partial) thermal equilibrium.

- First, as all LEED $I(E)$ data were recorded at low temperature ($\approx$100 K), the observed surface relaxation and thermal atomic MSD correspond to thermal equilibrium around 100 K.
- Second, any kind of diffusion freezes out at much higher temperatures. In particular, this holds for the *compositional* equilibration of the preferentially sputtered surface region with the faraway bulk. Since this process involves mass transport over at least a few nm [41], high annealing temperatures (here of the order of 1000 K) are required. In the present work, the state of compositional equilibrium was always reached as all samples were annealed to sufficiently high temperatures (see below) where the observed near-surface composition became independent of the annealing temperature altogether [28].
- Third, the diffusion processes that shape the near-surface order and segregation involve only a few atomic layers close to the surface. Due to their local nature, these processes are faster than "long-range" mass transport, and the

near-surface region is able to reach its own local equilibrium independent of whether the full long-range equilibrium with the bulk has been attained.

Conversely, the measured surface structure and composition profile discussed below correspond to the temperature at which short-range diffusion processes freeze out during quenching rather than to the annealing temperature necessary to establish "long-range" equilibrium. From Ref. [28], this freezing temperature can be inferred to range between 500 and 800 K. The findings reported below concerning equilibrium segregation and local order are expected to correspond to thermodynamic equilibrium at temperatures in this range and do not, for instance, reflect low temperature behavior.

For both $Fe_{0.97}Al_{0.03}(1\,0\,0)$ and $Fe_{0.85}Al_{0.15}(1\,0\,0)$, the equilibrium LEED patterns reported in previous work [25,26] are reproduced. The former shows a sharp, low background c(2×2) superstructure while the latter is characterized by a simple (1×1) arrangement. Its spots are also sharp, but there remains some diffuse background intensity near the half-order spot positions, indicating some short-range order of the surface even though the corresponding long-range order fails to develop. Interestingly, this diffuse intensity for $Fe_{0.85}Al_{0.15}(1\,0\,0)$ still bears some resemblance to the ordered half-order $I(E)$ curves of $Fe_{0.97}$-$Al_{0.03}(1\,0\,0)$, hinting to a common structural origin of both, despite the striking differences of the integer-order spectra measured from both surfaces (see Fig. 2).

For the quantitative LEED analysis of $Fe_{0.85}$-$Al_{0.15}(1\,0\,0)$, $I(E)$ curves were measured after annealing the sample at 1200 K. As mentioned above, the surface preparation of the clean

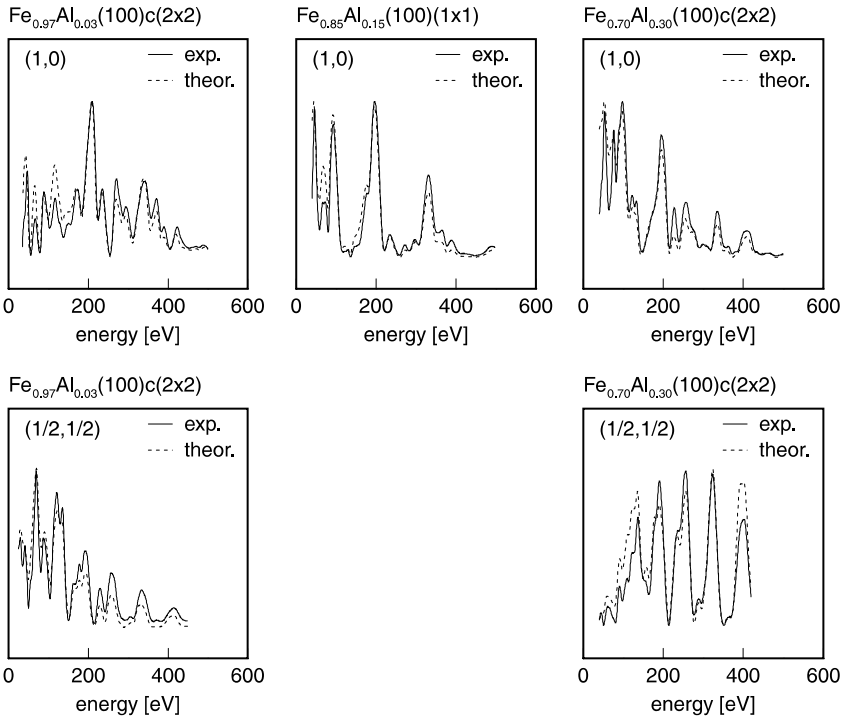

Fig. 2. Comparison of the LEED $I(E)$ spectra measured from $Fe_{0.97}Al_{0.03}(1\,0\,0)$-c$(2\times2)$ (left column), $Fe_{0.85}Al_{0.15}(1\,0\,0)$-$(1\times1)$ (center), and $Fe_{0.70}Al_{0.30}(1\,0\,0)$-c$(2\times2)$ (right column) with those calculated for the respective best-fit structural models. In each case, the $(1,0)$ beam is shown. For the c(2×2) phases, the curves for the $(\frac{1}{2},\frac{1}{2})$ beam are also depicted. The curves clearly reflect the structural differences between all three surface phases. That notwithstanding, there is excellent visual agreement between the experimental and best-fit curves for each phase.

$Fe_{0.97}Al_{0.03}(1\,0\,0)$ sample was limited to a temperature window below 1150 K. To ensure that contaminants did not influence the equilibrium surface structures observed from this sample, two separate $I(E)$ data sets were measured and analysed, one after annealing the sample to 960 K and one at 1120 K, just below the onset of S segregation. Both data sets agree quite closely ($R_P = 0.06$) and so yield very similar results in the quantitative analysis (discussed in the next section). However, the experiment–theory agreement that can be achieved for the fractional-order beams of the 1120 K data set is systematically worse than that for the 960 K data set. Moreover, the ratio of energy-averaged intensities between fractional and integer order beams is significantly lower for the 1120 K data ($I_{\text{frac}}/I_{\text{int}} = 0.28$ compared to 0.53 for the 960 K data), indicating that the overall surface order is lower for the 1120 K preparation. As we cannot fully exclude the possibility that this loss of order is related to the nearby onset of S segregation, the discussion of structural results below will focus on the 960 K preparation.

In accordance with the periodicity expected for $D0_3$ order, the $Fe_{0.70}Al_{0.30}(1\,0\,0)$ surface exhibits a $c(2\times 2)$ LEED pattern. For the $I(E)$ measurement, the surface was flashed to 1000 K to establish compositional equilibrium with the bulk. Then, the sample was cooled down slowly to below 100 K (≈10 min cooling time), leaving additional time for ordering in the $D0_3$ region of the phase diagram. As can be seen in Fig. 2, the $I(E)$ spectra measured from this surface are distinctly different from those found for $Fe_{0.97}Al_{0.03}(1\,0\,0)$-$c(2\times 2)$, i.e. the two phases must be of rather different atomic structure. On the other hand, the spectra for $Fe_{0.70}Al_{0.30}(1\,0\,0)$-$c(2\times 2)$ are quite similar to those found for the intermediate $c(2\times 2)$ phase identified on a preferentially sputtered and partially annealed FeAl(1 0 0) surface [28]. The latter was identified as a $D0_3$-ordered phase capped by a nearly pure layer of Al [27], so the equilibrium structure of $Fe_{0.70}Al_{0.30}(1\,0\,0)$ should be similar. The $c(2\times 2)$ pattern remains clearly visible up to a sample temperature of approximately 700 K where, consistent with the $D0_3 \leftrightarrow B2$ phase transition in the bulk, the periodicity reversibly switches to (1×1) order. Unfortunately, it is not possible to quantitatively investigate the equilibrium structure of the (1×1) state of the surface as $I(E)$ measurements at high temperature are hampered by thermal diffuse scattering, and quench times are too long to prevent $D0_3$ reordering while cooling down.

In summary, three distinctly different surface terminations on the three samples investigated are found which each occur in compositional equilibrium with the underlying bulk crystal. Section 4 will deal in detail with the atomic arrangement responsible for the observed superstructures.

4. Surface order and atomic structure

4.1. $Fe_{0.97}Al_{0.03}(1\,0\,0)$-$c(2\times 2)$

In order to obtain some basic information on the structure and order of $Fe_{0.97}Al_{0.03}(1\,0\,0)$-$c(2\times 2)$, it would be worthwhile to investigate this surface by STM, exploiting a possible chemical resolution of the elements in the topmost layer, and LEIS. While not performed for $Fe_{0.97}Al_{0.03}$ itself, such investigations were carried out for a transient $c(2\times 2)$ superstructure that appears on partially annealed $Fe_{0.85}Al_{0.15}(1\,0\,0)$. Ref. [28] shows clearly that the latter surface phase is structurally equivalent to $Fe_{0.97}Al_{0.03}(1\,0\,0)$-$c(2\times 2)$ in compositional equilibrium. In particular, the order properties of both should therefore agree quite closely. The STM image of $Fe_{0.85}Al_{0.15}(1\,0\,0)$-$c(2\times 2)$ in Fig. 3 shows that topmost layer is indeed dominated by large areas forming a $c(2\times 2)$ superstructure of nearly perfect order. This superstructure can be visually distinguished from a (1×1) arrangement by the antiphase boundary associated with the (untypically large) defect near the image center. As the average apparent corrugation of the surface in STM, lying between 0.15 and 0.20 Å, is quite small, the $c(2\times 2)$ periodicity is most likely caused by an ordered arrangement of Fe and Al atoms. However, protrusions that clearly indicate the presence of "atoms" can only be seen on one of the two $c(2\times 2)$ sublattices, so that, strictly, the observed surface structure could still be due to an ordered arrangement of vacancies and adatoms. As AES

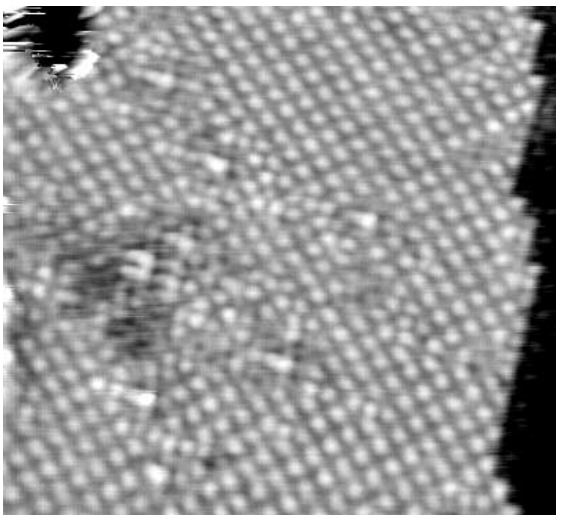

Fig. 3. Room temperature STM image (100×100 Å^2, $U_{\text{sample}} = -0.5$ mV, $I = 2.1$ nA) of the preferentially sputtered and partially annealed $Fe_{0.85}Al_{0.15}$(1 0 0)-c(2×2) surface ($T_{\text{anneal}} \approx 700$ K) which has the same surface structure as $Fe_{0.97}Al_{0.03}$(1 0 0)-c(2×2) [28]. Its ordered parts show a nearly perfect c(2×2) atomic arrangement, visually distinguishable from a (1×1) structure by an antiphase boundary that is associated with the untypically large defect near the image center.

measurements clearly establish the segregation of Al to the surface, these adatoms could only be Al. LEIS spectra taken in the [0 1 1] azimuth show the presence of both species but, in the presence of top layer vacancies, the second layer would also contribute to this signal so that this method cannot safely distinguish between both models without a more quantitative interpretation. In total, we conclude from STM, AES and LEIS that the top layer consists of quite close to 50% Al, and that its remaining sites are most likely occupied by Fe, although a vacancy model cannot strictly be ruled out by these methods alone.

In line with these results, two structural models were tested in the quantitative LEED analysis of $Fe_{0.97}Al_{0.03}$(1 0 0)-c(2×2). Based on the near-perfect c(2×2) superstructure that, in STM, dominates the surface, the analysis was restricted to a fully ordered top layer composed of equal fractions of Al and either vacancies or Fe. Note that the c(2×2) symmetry of the topmost layer, in principle, creates two independent sublattices there as well as in the third, fifth, etc. atomic layers. In order to maintain consistency with the notation used later for the $D0_3$ structure, we define sublattice 1 of the third layer to reside below sublattice 2 of the topmost layer, and vice versa. The free parameters of the LEED structural analysis were the chemical composition c_2, c_3^1 and c_3^2, and c_4 of the second, third, and fourth layer, respectively, as well as the vertical atomic positions in the top four layers. Lower-lying layers were fixed to their bulk-like composition and geometry. Tests for the fifth layer showed that this assumption holds very well within the limits of error.

Already after the first tensor LEED reference calculation and optimization, the adatom-vacancy model can be ruled out as it yields average Pendry R-factors above 0.35 only while the model of a mixed ordered top layer yields $R_P = 0.10$ in the analogous step. So, the topmost layer of $Fe_{0.97}$-$Al_{0.03}$(1 0 0)-c(2×2) really consists of an ordered arrangement of Al and Fe atoms. The agreement achieved between experimental $I(E)$ curves and the calculated best-fit data after further refinement demonstrates that this model accurately describes the surface structure. The average Pendry R-factor amounts to $R_P = 0.083$ for a total data base width of $\Delta E = 2858$ eV. The fit quality for integer ($R_P = 0.075$, $\Delta E = 2012$ eV) and fractional order beams ($R_P = 0.106$, $\Delta E = 846$ eV) is similar. The favorable comparison between experimental and theoretical $I(E)$ curves is demonstrated for the $(1,0)$ and $(\frac{1}{2},\frac{1}{2})$ beams in the left column of Fig. 2. Table 1 (left column) summarizes the best-fit structural parameters achieved for $Fe_{0.97}Al_{0.03}$(1 0 0)-c(2×2) which are visualized in Fig. 4. A look at the ratio of energy-averaged intensities between fractional and integer order beams further strengthens the assumption of an almost perfectly ordered top layer: the measured $I_{\text{frac}}/I_{\text{int}} = 0.53$ is very close to the calculated value of 0.63 for the best-fit model, indicating a rather defect-free superstructure in experiment.

Except for the Al segregation and chemical ordering in the topmost layer, the surface shows surprisingly little differences from a truncated bulk model. The only obvious deviation from the bulk stoichiometry occurs on that third layer sublattice site ($15 \pm 12\%$ Al) which is the second nearest neighbor to the top layer Fe sublattice site.

Table 1
Best-fit parameters of the LEED $I(E)$ analyses for $Fe_{0.97}Al_{0.03}(1\,0\,0)$-c$(2\times2)$, $Fe_{0.85}Al_{0.15}(1\,0\,0)$-$(1\times1)$ and $Fe_{0.70}Al_{0.30}(1\,0\,0)$-c$(2\times2)$ as described in the text[a]

	$Fe_{0.97}Al_{0.03}(1\,0\,0)$-c$(2\times2)$	$Fe_{0.85}Al_{0.15}(1\,0\,0)$-$(1\times1)$	$Fe_{0.70}Al_{0.30}(1\,0\,0)$-c$(2\times2)$
R_P	0.083	0.069	0.078
$a=2d_b$ (Å)	2.865 ± 0.012	2.887 ± 0.013	2.895 ± 0.011
$\Delta d_{12}/d_b$ (%)	-1.4 ± 1.4	-7.1 ± 1.5	-12.3 ± 1.2
$\Delta d_{23}/d_b$ (%)	$+1.7\pm1.0$	0.0 ± 0.7	$+3.2\pm0.7$
$\Delta d_{34}/d_b$ (%)	-0.3 ± 1.0	$+1.4\pm0.7$	-0.6 ± 0.7
$\Delta d_{45}/d_b$ (%)	$+0.7\pm1.0$	-0.7 ± 0.7	-0.7 ± 0.7
b_1 (Å)	0.06 ± 0.04 (Al out)	0.05 ± 0.04 (Al out)	0.01 ± 0.015
b_3 (Å)	0.01 ± 0.01		0.05 ± 0.01 (Al out)
c_1^1(Al)/c_1^2(Al) (%)	100/0 (fixed)	75 (fixed)	$90\pm5/90\pm5$
c_2(Al) (%)	0 ± 12	5 ± 7	15 ± 10
c_3^1(Al)/c_3^2(Al) (%)	$5\pm8/15\pm12$	20 ± 5	$25\pm10/90\pm10$
c_4(Al) (%)	5 ± 10	15 ± 5	5 ± 10
v_1(Al) (Å)	0.12 ± 0.04	0.17 ± 0.03	0.11 ± 0.03
v_1(Fe) (Å)	0.12 ± 0.03	$0.16^{+0.09}_{-0.04}$	
v_2 (Å)	0.10 ± 0.02	0.13 ± 0.01	0.10 ± 0.02
v_b (Å)	0.06 ± 0.03	0.10 ± 0.02	0.08 ± 0.03 (Al) 0.07 ± 0.03 (Fe)

[a] The error limits given are determined from the variance of R_P by single-parameter R-factor scans. The interlayer relaxations given are values averaged over different sublattices or, for $x=0.15$, the weighted average over both elements. Individual concentrations c_i^1 and c_i^2 are given for c(2×2) sublattices of layers as described in the text.

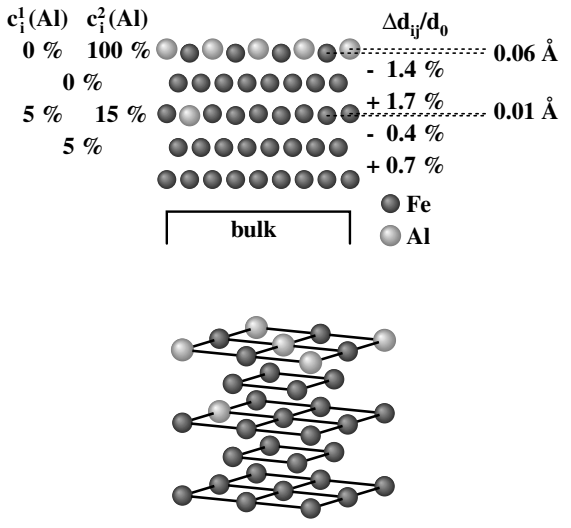

Fig. 4. Best-fit structural model for $Fe_{0.97}Al_{0.03}(1\,0\,0)$-c$(2\times2)$. Sublattices of layers with c(2×2) periodicity are denoted 1 and 2, respectively, where sublattice 2 of the third layer is situated perpendicularly below sublattice 1 of the top layer.

However, when also taking parameter correlations into account, the Al enrichment found there is not outside the limits of error of our analysis as defined by the variance of the Pendry R-factor. So, this point remains uncertain: it may be regarded as a hint towards a possible subsurface ordering that occurs but could still be due to an artifact of the analysis. The best-fit lattice parameter amounts to $a=2.865\pm0.012$ Å, equivalent to a bulk interlayer spacing of $d_b=1.433$ Å. The changes in the average near-surface interlayer distances compared to this value are very small (just outside the error limits given) but adhere to the usual oscillatory scheme ($\Delta d_{12}/d_b=-1.4\pm1.4\%$, $\Delta d_{23}/d_b=+1.7\pm1.0\%$, no significant relaxation below). Additionally, the topmost layer shows a small atomic buckling of $b_1=0.06$ Å which places its Fe atoms at nearly the same position as that found for the clean Fe(1 0 0) surface [42] while the Al atoms reside further out. Finally, the bulk atomic MSD determined in the analysis, $v_b=0.06\pm0.03$ Å, is in good agreement with the value of 0.07 Å expected for

pure Fe ($\Theta_D = 465$ K [43]), and the values for the top and second layer are enhanced as expected.

4.2. $Fe_{0.85}Al_{0.15}(1\,0\,0)$-$(1 \times 1)$

As mentioned, the LEED pattern of the well-annealed $Fe_{0.85}Al_{0.15}(1\,0\,0)$ surface shows some diffuse intensities indicative of local $c(2 \times 2)$ ordering but, in contrast to $Fe_{0.97}Al_{0.03}(1\,0\,0)$, lacks long-range order. The observation of a (1×1) LEED pattern is an indication for Al segregation beyond half a monolayer as discussed earlier [26]. In order to determine this quantity more precisely, we applied both LEIS and chemically resolved STM. Fig. 5(a) shows a typical LEIS spectrum from $Fe_{0.85}Al_{0.15}(1\,0\,0)$-$(1 \times 1)$. With the peak at 880 eV stemming from Fe and that at 750 eV from Al, the presence of both elements in the topmost layer is clearly established. In order to achieve a quantitative result, similar LEIS spectra were also measured for the intermediate $Fe_{0.85}Al_{0.15}(1\,0\,0)$-$c(2 \times 2)$ phase mentioned above (cf. Fig. 3), the topmost layer of which contains equal amounts of Al and Fe according to STM and LEED. Using its integrated LEIS peak areas for calibration and assuming composition-independent sensitivity factors for both elements, the topmost layer composition of $Fe_{0.85}Al_{0.15}(1\,0\,0)$-$(1 \times 1)$ was determined to be 75% Al.

Under certain tip conditions, STM images show clear chemical contrast between both elements. In Fig. 5(b), the minority species (Fe) appear as protruding atoms while the majority species (Al) appear as dark indentations, i.e. the surface shows Al anticorrugation at the imaging conditions used, with an average height difference of 0.21 Å between Al and Fe atoms. The quantitative evaluation of several STM images by atom counting yields a top layer composition of 76% Al, in excellent agreement with the above LEIS result. Moreover, Fig. 5(b) gives insights into the local surface order. It turns out that the Fe atoms form small patches of local $c(2 \times 2)$ order. These hardly ever contain Fe atoms on adjacent top layer lattice sites, indicative of the effective repulsion between bcc second nearest Fe neighbors. Apparently, no such repulsive force is encountered between third nearest neighbors since, otherwise, no local $c(2 \times 2)$ ordering could occur.

In the LEED analysis, the top layer concentration was kept fixed at 75% Al as determined by LEIS and STM in order to avoid the correlation with element-dependent atomic MSD there (see Section 2). The main free parameters in the analysis were thus the vertical positions of the top four layers and the chemical composition of the second through fourth layers, keeping all deeper layers fixed at their bulk position and composition. As

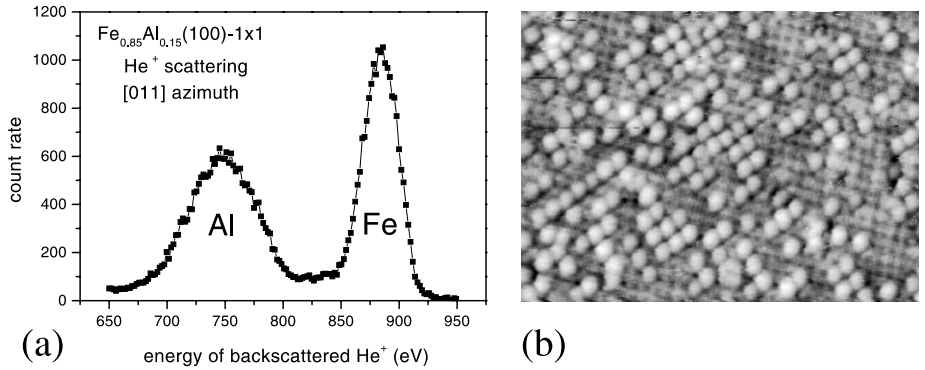

Fig. 5. (a) LEIS spectrum of $Fe_{0.85}Al_{0.15}(1\,0\,0)$-$(1 \times 1)$ ([0 1 1] azimuth), indicating a top layer Al concentration of 75% Al. The LEIS signal was calibrated against the signal obtained from the intermediate $Fe_{0.85}Al_{0.15}(1\,0\,0)$-$c(2 \times 2)$ phase. (b) Room temperature STM image (100×83 Å^2, $U_{sample} = -6$ mV, $I = 0.46$ nA) of the well-annealed $Fe_{0.85}Al_{0.15}(1\,0\,0)$-$(1 \times 1)$ surface ($T_{anneal} \approx 1100$ K). Clear chemical contrast between Fe (protruding atoms) and Al (dark indentations) is achieved (average apparent height difference between Fe and Al: 0.21 Å), showing the surface to consist of 76% Al. The surface shows clear local ordering as hardly any Fe atoms reside immediately next to one another, forming small $c(2 \times 2)$ patches instead.

for $Fe_{0.97}Al_{0.03}$(1 0 0)-c(2 × 2), tests showed no deviations of the fifth layer from bulk order. Although the (1 × 1) structural model does not allow for an ordered buckling of the topmost layer, element-dependent atomic positions for Fe and Al are likely to occur and thus were taken into account within the tensor LEED approximation, using the method described in Refs. [31,44].

Table 1 (second column) summarizes the best-fit parameters obtained in the LEED analysis of $Fe_{0.85}Al_{0.15}$(1 0 0). The model is depicted in Fig. 6. Again, the agreement achieved between calculated and experimental spectra is excellent, characterized by $R_P = 0.069$ for an overall $I(E)$ data base width of 2019 eV (for the $(1,0)$ beam, the visual comparison between experiment and theory is given in the middle column of Fig. 2). With an Al depleted second layer following the enriched very surface, the composition profile is oscillatory but strongly damped into the crystal. Likewise, geometrical relaxations comprise only few atomic layers. The topmost spacing shows a stronger contraction than observed for the 3 at.% Al sample, amounting to $\Delta d_{12}/d_b = -7.1 \pm 1.5\%$ ($d_b = 1.443 \pm 0.007$ Å). The element-dependent disordered buckling of the topmost layer, $b_1 = 0.05$ Å with Al displaced out of the crystal, is essentially the same as for $Fe_{0.97}Al_{0.03}$(1 0 0)-c(2 × 2). It is also significant in view of its single-parameter error bars (±0.04 Å). However, when restricting both atoms to the same atomic position in the topmost layer and readjusting all other parameters, the best achievable R-factor remains within the variance level of the overall best fit. As a consequence, from LEED alone we cannot decide whether or not the small observed buckling is real. Last, the fitted atomic MSD show a consistent trend, increasing from the bulk via the second to the topmost layer. They appear to be enhanced compared to case of $Fe_{0.97}Al_{0.03}$(1 0 0)-c(2 × 2) though the ranges of error overlap.

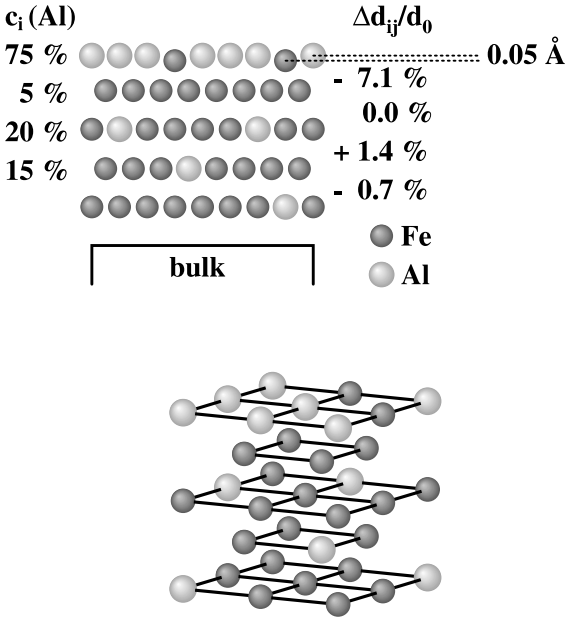

Fig. 6. Best-fit structural model for $Fe_{0.85}Al_{0.15}$(1 0 0)-(1 × 1).

4.3. $Fe_{0.70}Al_{0.30}$(1 0 0)-c(2 × 2)

The $I(E)$ spectra for $Fe_{0.70}Al_{0.30}$(1 0 0)-c(2 × 2) in compositional equilibrium with the bulk are very similar to those of a partially annealed $Fe_{0.53}Al_{0.47}$(1 0 0) surface described earlier [27,28]. The structural model presented for the latter surface consists of a nearly complete Al top layer with a $D0_3$ ordered bulk underneath reaching beyond the depth accessible to quantitative LEED. Thus, for the present work, we restricted our analysis to this model [27] with only the parameter values readjusted but no different model types considered.

An ideal (1 0 0) $D0_3$ bulk sample consists of an alternating sequence of pure Fe and mixed Fe–Al layers in c(2 × 2) order (see Fig. 1). So, there are two inequivalent sublattices for the topmost, third, fifth etc. layer, that either contain Fe (which we define as sublattice 1) or Al (sublattice 2). Note that, using this convention, sublattice 2 of layer $i+2$ is situated perpendicularly below sublattice 1 of layers i (for odd i), and vice versa. In a $Fe_{0.70}Al_{0.30}$ bulk crystal, the Al atoms exceeding the ideal Fe_3Al stoichiometry are incorporated in form of substitutional structural defects on Fe sublattice sites of the mixed layers [45], i.e. $c_i^1 = 20$ at.% Al for all mixed layers in the bulk. During the structural analysis, all geometric and chemical degrees of freedom of the top four layers were adjusted including the occupation of sublattices with antisite atoms. This allows for disorder both

in sublattices of layers (in particular, the possibility of a top layer made up only by Al atoms) and in layers purely consistent of Fe in the $D0_3$ structure. As in the other cases, tests for the fifth layer showed no detectable deviation from the expected bulk-like order (with 20% Al occupying the Fe sublattice of that layer) and geometry and so could be excluded from the search procedure.

Again, the best fit achieved in the analysis is excellent ($R_P = 0.078$ with $\Delta E = 3105$ eV). Moreover, the fit quality is equally good for integer ($R_P = 0.071$, $\Delta E = 2058$ eV) and fractional order beams ($R_P = 0.094$, $\Delta E = 1047$ eV), indicating a reliable description of all ordered parts of the surface by our model. As expected, the best-fit structure as summarized in Table 1 (third column) and visualized in Fig. 7 agrees quite well with that of $Fe_{0.53}Al_{0.47}(1\,0\,0)$-c$(2\times 2)$ [27]: the top layer consists mainly of Al, and the region below shows $D0_3$ order. Interestingly, there are some indications for substitutional disorder in the surface region beyond the expected, bulk-like structural defects. According to the fit, the topmost layer is not pure Al but contains around 10% Fe, equally

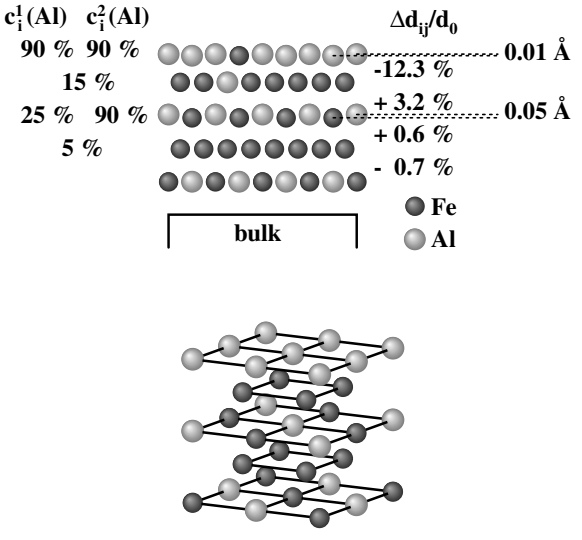

Fig. 7. Best-fit structural model for $Fe_{0.70}Al_{0.30}(1\,0\,0)$-c$(2\times 2)$. The inequivalent sublattices of each mixed layer are denoted 1 (Fe in ideal $D0_3$) and 2 (Al in ideal $D0_3$) respectively, with sublattice 2 of layer $i+2$ situated perpendicularly below sublattice 1 of layer i (for odd i). The $D0_3$ structure thus also allows for a buckling in the Al-enriched topmost layer.

distributed on both sublattices. Furthermore, the second layer holds a relatively large amount of antisites (15% Al), and the third layer shows small deviations from its expected bulk-like order. The best-fit lattice parameter amounts to $a = 2.895 \pm 0.011$ Å equivalent to an interlayer spacing of $d_b = 1.448$ Å. The topmost interlayer spacing is strongly contracted ($\Delta d_{12}/d_b = -12.3 \pm 1.2\%$), accompanied by an expansion of the average second interlayer spacing ($\Delta d_{23}/d_b = 3.2 \pm 0.7\%$). While there is no positional difference between the inequivalent sublattices of the top layer, the influence of the surface is apparently "felt" in the third layer where a small buckling of 0.05 ± 0.01 Å occurs (with the Al site lying closer to the topmost layer). Possibly, the modified next nearest neighbor bond between surface Al and third layer Fe manifests itself in the latter layer rather than at the very boundary to the vacuum. Again, atomic MSD were adjusted independently for bulk (Fe and Al separately), second and topmost layer atoms, indicating equal values for both elements in the bulk and increased ones in the second and topmost layer, close to those encountered for well-annealed $Fe_{0.97}Al_{0.03}(1\,0\,0)$ and $Fe_{0.53}Al_{0.47}(1\,0\,0)$ [24]. We also attempted to determine a possible dependence of the atomic positions in the topmost and third layer on the element occupying that site. However, the influence of these parameters on the fit quality turned out to be entirely negligible, i.e. elemental positions are equal within our limits of error.

Certainly, the most unusual feature of $Fe_{0.70}Al_{0.30}(1\,0\,0)$-c$(2\times 2)$ is the presence of substitutional defects in the surface region beyond those expected in the bulk. Possibly, this disorder is induced by the mere presence of a free surface, although the mechanism behind it remains unclear in the present case. However, before attempting a further interpretation of this phenomenon, it is worthwhile to investigate its overall influence in the $I(E)$ analysis. For comparison, we reperformed the entire analysis with all chemical parameters fixed at their bulk values, additionally requiring the top layer to consist of 100% Al. It turns out that this approach yields a best fit R-factor of $R_P = 0.092$, only slightly worse than the agreement obtained in the "full" analysis above. Though technically, bulk-like order is still outside the limits of error

(given by an extremely low R-factor variance of 0.009), the comparison demonstrates that the fit is not extremely sensitive to the observed extent of disorder. In view of the many additional parameters involved, we feel unable to decide whether the observed stoichiometric deviations from the ideal $D0_3$ structure are real or an artifact of the fitting procedure. In any case, our analysis yields no indication of *excessive* deviations from an ideal $D0_3$-ordered structure capped by a single atomic layer of Al.

5. Discussion

The structural information obtained for the three surfaces under investigation provides a sound basis to discuss the development of the structure, composition and order of (1 0 0) oriented Fe–Al alloy surfaces with increasing bulk Al content. In the following, we will first highlight some general trends when crossing the Fe-rich region of the Fe–Al phase diagram (Fig. 1), and then focus on the relation between near-surface order and Al surface segregation.

5.1. Surface structural trends with growing Al content

Concerning the geometric structure, the most striking systematic feature of $Fe_{1-x}Al_x(1\,0\,0)$ is the development of its average topmost interlayer spacing d_{12} with growing bulk Al content (Fig. 8(a)). Whilst relaxations of deeper spacings are relatively small, the relaxation Δd_{12} of the top spacing can assume rather large values. It starts out with hardly any contraction at all, even less than $\Delta d_{12}/d_b = -5\%$ of Fe(1 0 0) [42], and then continuously develops towards the strong contraction of -14.6% observed for near-stoichiometric FeAl(1 0 0) [23,24]. So, as pointed out earlier [23], although some (1 0 0) surfaces of bcc-based materials do display large relaxations of d_{12} (e.g. -12% for $Mo_{0.75}Re_{0.25}(1\,0\,0)$ [46], -11% for Ta(1 0 0) [47], -7% for V(1 0 0) [48]), FeAl shows the strongest contraction observed as yet. Of course, the mere chemical change in the topmost layer from 0% Al (pure Fe(1 0 0)) to 100% Al might be responsible for the observed development of d_{12}. However, this scenario is unlikely as d_{12} continues to contract even after a practically full Al layer has been reached for $Fe_{0.70}Al_{0.30}$. Instead, the observed trend could be driven by electronic changes in the second layer. Of course this is rather speculative, but there are some mechanisms one could conceive to explain such behavior. For example, the modified bonding may come about locally via the continuously changing charge density in the third layer due to the increase in Al content there, and/or globally, e.g. via the decreasing magnetic moment of the second layer Fe atoms with increasing overall Al content (indicated by the decrease of the ferromagnetic T_c between 0 and 30 at.% Al [14]).

In our analyses, we also determined the lattice spacing a for $Fe_{1-x}Al_x$ within the depth accessible

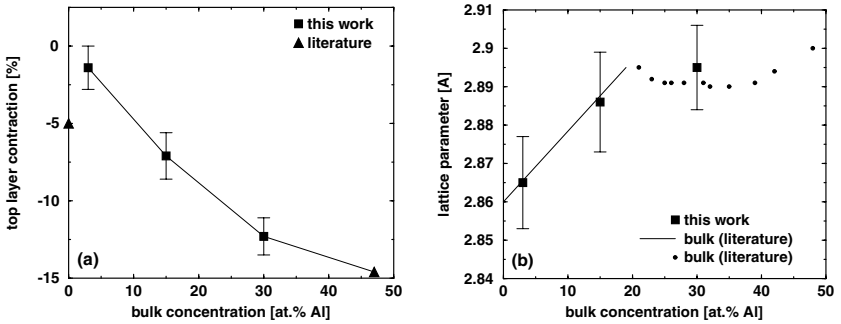

Fig. 8. (a) Development of the topmost interlayer spacing with growing bulk Al content. Values not from this work are taken from Ref. [42] (Fe) and Ref. [24] ($Fe_{0.53}Al_{0.47}$). (b) Best-fit lattice parameter as a function of bulk Al content compared to bulk values [49] corrected for temperature [50].

to LEED. In general, a depends on the exact alloy composition and on temperature. In many cases, accurate literature values are hard to find, making a direct determination by LEED desirable. For $Fe_{1-x}Al_x$, measurements of a at room temperature exist [14,49] that suggest a change of a by only about 1% between 0% and 50% Al. Our observations are consistent with this trend, but for a quantitative comparison, the data of Refs. [14,49] require some temperature corrections since our $I(E)$ data was measured slightly below 100 K. As suitable values for Fe–Al alloys could not be found in the literature, we estimated this correction from the known thermal expansion coefficient of Fe at low temperature [50]. The agreement between the lattice parameters obtained in the present work and the temperature-corrected data of Ref. [49] (shown in Fig. 8(b)) is remarkable – both sets lie much closer together than could be expected from our single-parameter error limits. As best-fit lattice parameters in LEED depend crucially on the use of the correct energy-dependent inner potential [39], our results imply a high accuracy of the ab initio energy-dependent inner potentials [40] used in the analysis (see Section 2).

A third point concerns the local geometry of disordered alloys. While the bulk atomic MSD of 0.06 Å found for $Fe_{0.97}Al_{0.03}$ compares favorably to the value expected for bulk Fe from a simple Debye model, the MSD of 0.10 Å found for $Fe_{0.85}Al_{0.15}$ is noticeably enhanced. In principle, the same finding holds also for the top and second layer. Although the overall sensitivity of our fit to these quantities is low, this behavior appears to be systematic. The most likely explanation is a contribution of static displacive disorder that adds to the usual thermal MSD at this composition. In fact, such static displacive disorder has been observed in careful, temperature-dependent γ-ray and neutron diffraction experiments performed with a $Fe_{0.80}Al_{0.20}$ random alloy sample [51], suggesting an average MSD of 0.092 Å with 0.074 Å due to thermal and ground-state atomic motion and 0.055 Å due to static displacements at 77 K. From our data, it seems that these large static MSD only develop well within the A2 random alloy region of the phase diagram. For $Fe_{0.70}Al_{0.30}$, the best-fit atomic MSD are again lower and consistent with what would be expected from mere thermal vibrations. Obviously, the development of long-range order eliminates the need for local lattice relaxations that accommodate the varying bonding geometry in the disordered phase.

5.2. Segregation and ordering in (1 0 0) oriented Fe–Al alloys

As mentioned in the introduction, the main aim of the present work is the study of the interplay of ordering interactions and surface segregation on a given lattice in a binary alloy. $Fe_{1-x}Al_x(1\,0\,0)$ surfaces turn out to be well suited for this purpose for several reasons:

- The system is clearly an ordering one, shown by the phase diagram as well as by measured [15] and calculated [16] effective pair interactions in the random alloy region. These effective pair interactions (which indicate by how much the heterogeneous occupation of two respective lattice sites is favored over the average homogeneous occupation) are tabulated in Fig. 9, together with a drawing that shows the location of the respective pairs on the bcc lattice. Qualitatively, only nearest (NN) and second nearest neighbor (2NN) terms are of appreciable magnitude, while further-reaching interactions play a much smaller role.
- There is a clear tendency towards Al segregation in this system [12].
- In (1 0 0) atomic planes of the bcc lattice there are no NN bonds (Fig. 9). So, the NN of a (1 0 0) surface atom are located in the second atomic layer, and the segregation of the minority component Al to the very first layer competes with the weaker in-plane 2NN forces only. These turn out to be strong enough to shape the observed surface order on the bcc lattice, but the lattice itself remains intact, i.e. no strong geometric reconstructions occur as observed, e.g., on other low-index FeAl surfaces [18–20].

Surface segregation in random alloys is driven by the segregation enthalpy ΔH_{seg}, i.e. the energy gained when one atom in the topmost layer is exchanged with the another of a different kind from

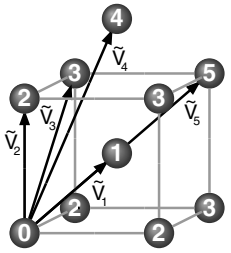

Ref.	$\tilde{V}_1$	$\tilde{V}_2$	$\tilde{V}_3$	$\tilde{V}_4$	$\tilde{V}_5$	[meV]
Sanchez et al.	23.7	7.1	-0.9	0.3	1.6	
Staunton et al.	48.4	27.6	-1.7	-3.4	0.0	

Fig. 9. Left: location of NN, 2NN etc. atoms in the bcc lattice, shown relative to the lower left front atom (no. 0). Note that a (1 0 0) plane contains only 2NN pairs, the NN are located in the adjacent planes. Right: effective pair interaction energies for bulk $Fe_{0.80}Al_{0.20}$ as obtained by Sanchez et al. [15] from neutron scattering data at 1273 K and calculated by Staunton et al. [16] at 500 K.

a bulk lattice site. On the other hand, surface segregation is usually reduced by entropy, i.e. it decreases with rising temperature. Based on these factors only, the simplest model for surface segregation (the Langmuir–McLean model [17,52]), predicts a smooth rise of the surface concentration c_1 with the bulk concentration of the segregating element, x:

$$\frac{c_1}{1-c_1} = \frac{x}{1-x}\exp\left(-\frac{\Delta H_{\mathrm{seg}}}{\mathrm{k}T}\right)$$

In particular, this model assumes ideal mixing and no short-range order whatsoever, and clearly is not applicable in our case. Instead of a smooth increase of c_1 with x, we observe a fast increase of c_1 to 50% Al already at $x = 0.03$, and then a much slower increase to a full Al top layer (which is nearly reached at $x = 0.30$). However, our observations may qualitatively be explained in terms of a similar model when taking the observed surface order directly into account. As mentioned, Al segregation to the $Fe_{1-x}Al_x(1\,0\,0)$ surface is directly opposed by in-plane bcc 2NN pair interactions between Al atoms. Segregation initially circumvents these repulsive interactions by filling only sites that do not yet have an Al atom as an in-plane 2NN. Thus, the top layer is effectively divided into two inequivalent sublattices of $c(2\times 2)$ periodicity. Apparently, this first step of segregation is already complete for $Fe_{0.97}Al_{0.03}$, with one full Al sublattice and no 2NN Al pairs in the surface plane. The segregation enthalpy ΔH_{seg} is also strong enough to overcome entropy at the temperature of local equilibrium (which, as mentioned before, should correspond to the temperature where local diffusion freezes out in the quenching process). The remaining top layer sites are populated with Al in a second step only. This filling is a gradual process: c_1(Al) amounts to 75% in the top layer of $Fe_{0.85}Al_{0.15}(1\,0\,0)$, and a (nearly) complete Al termination only develops for much higher bulk Al content ($x = 0.30$ or above). Consistently, the lateral short-range order for $Fe_{0.85}$-$Al_{0.15}(1\,0\,0)$ as observed by STM demonstrates that in-surface 2NN interactions are still effective. Apparently, in this regime, they compete with the segregation of Al and create an equilibrium state of the surface that depends sensitively on the Al content of the underlying bulk. In order to fill the second sublattice with Al, segregation must work against the repulsive force of four 2NN Al atoms in the top layer. So, the effective segregation enthalpy for the second sublattice is reduced to approximately $\Delta H_{\mathrm{seg}}^{\mathrm{eff}} \approx \Delta H_{\mathrm{seg}} - 4\tilde{V}_2$.

In order to obtain a rough quantitative estimate of the magnitude of $\Delta H_{\mathrm{seg}}^{\mathrm{eff}}$ we can make use of the experimental result of $c_1 = 75\%$ Al at $x = 0.15$, indicating the second sublattice to be occupied by 50% Al. Inserting this value into the Langmuir–McLean formula (now used for the second sublattice only) and assuming a temperature of 700 K for the local thermal equilibrium, $\Delta H_{\mathrm{seg}}^{\mathrm{eff}}$ turns out to be of the order of 0.1 eV. As expected, the effective segregation enthalpy noticeably exceeds the 2NN interactions that oppose a segregation (see the table included in Fig. 9). On the other hand, it is not extremely large compared to at least the theoretically determined $\tilde{V}_2$ [16]. The distinct splitting of the segregation process into two sublattices that we observe is a direct consequence of the approximate balance between both segregation and in-surface pair interactions. If the latter were

considerably weaker than ΔH_{seg}, no two-step segregation due to local ordering would occur, leading to the usually observed segregation behavior in random alloys (e.g. $Mo_{1-x}Re_x$ [46]) instead. In contrast, stronger in-surface pair interactions would prevent a segregation beyond a filled first sublattice entirely. The fcc-based alloy $Ni_{0.90}Al_{0.10}$(1 1 1) appears to be an example for such behavior: its top layer contains 25% Al [53,54], a stoichiometry that just avoids Al–Al NN if a p(2 × 2) arrangement is formed [55]. However, the in-plane ordering interactions opposing a further Al segregation in the Ni–Al system are of the order of 0.1 eV [53], and no further Al segregation occurs for higher bulk Al content – a bulk-like termination of Ni_3Al(1 1 1) is observed [56,57].

In parallel to Al segregation and ordering in $Fe_{1-x}Al_x$(1 0 0), short-range order also develops perpendicularly to the surface, induced by the strong top-layer Al enrichment. The oscillatory concentration profile found for $Fe_{0.85}Al_{0.15}$(1 0 0) reflects the ordering NN interactions between subsequent atomic layers, and similar surface-induced local ordering (the same that shapes the B2-type long-range order for higher Al contents) has been observed for numerous other alloy systems [17]. In the Fe–Al system, one would moreover expect the lateral short-range atomic arrangement in the top layer to induce the same order in the third layer through 2NN interactions perpendicular to the surface. Unfortunately, our LEED analyses are not sensitive to this kind of local ordering. The effect is too small for $Fe_{0.97}Al_{0.03}$(1 0 0), and the LEED pattern of $Fe_{0.85}Al_{0.15}$(1 0 0) displays only (1 × 1) spots which are quite insensitive to such ordering.

Since the observed order of Fe–Al(1 0 0) surfaces clearly reflects pair interactions similar to those in the bulk, the question arises whether the formation of bulk order also leaves its imprint on Al segregation to the surface. The answer is best given by considering $Fe_{0.70}Al_{0.30}$(1 0 0), where bulk $D0_3$ order is fully established according to the phase diagram. Here, we observe a nearly pure Al top layer that does not even show any significant buckling of its two $D0_3$ sublattices, indicating that bulk order fails to have any noticeable consequences in the surface itself. Instead, we find that the presence of a surface might even affect the near-surface ordering interactions, as our fit hints to some substitutional disorder in $Fe_{0.70}Al_{0.30}$(1 0 0). This possible weakening of pair interactions near the surface could be explained by changes in bonding (as manifest e.g. in the strong relaxation of the topmost interlayer spacing). In any case, yet, the effect is not very strong since the observed degree of substitutional disorder is at the limits of sensitivity of our analysis.

6. Conclusion

In summary, we have investigated the interrelation between segregation and local order at (1 0 0) oriented surfaces of the binary system Fe–Al in the Fe-rich regime. Our study reveals that the segregation of Al is divided into two regimes by in-surface 2NN ordering interactions similar to those in the bulk. For very low Al contents, an ordered, chessboard-like c(2 × 2) arrangement of Fe and Al atoms forms in the very surface layer, indicating the fast filling of those surface sites that do not (yet) have Al 2NN. As the in-surface 2NN repulsion between Al atoms is not strong enough to prevent Al segregation entirely, the top layer Al fraction increases gradually on the remaining surface sites with increasing Al bulk concentration, eventually leading to a nearly complete termination by Al in the $D0_3$ region of the phase diagram. The top layer Al enrichment induces an oscillatory compositional profile decaying towards the bulk. It is due to bulk-like NN interactions and may be interpreted as precursor of $D0_3$ and B2 order. Although the relaxation of the topmost interlayer spacing increases continuously with bulk Al content, the surface adheres to its bcc arrangement and does not reconstruct geometrically, making it an ideal model system for the study of order and segregation on a simple lattice.

Acknowledgements

We are grateful to Dr. H. Viefhaus (Max-Planck-Institut für Eisenforschung, Düsseldorf) for providing Fe–Al single crystals of excellent

quality. Moreover, we are indebted to Prof. J. Rundgren (Stockholm) for making his work on energy-dependent inner potentials available to us. Support through Deutsche Forschungsgemeinschaft (German Science Foundation, DFG) and the Fonds zur Förderung der Wissenschaftlichen Forschung (Austrian Science Foundation) is also gratefully acknowledged.

References

[1] G. Sauthoff, Intermetallics, VCH, Weinheim, 1995.
[2] N.S. Stoloff, Mat. Sci. Engng. A 258 (1998) 1.
[3] C.T. Liu, E.P. George, P.J. Maziasz, J.H. Schneibel, Mat. Sci. Engng. A 258 (1998) 84.
[4] N.S. Stoloff, C.T. Liu, Intermetallics 2 (1994) 75.
[5] H. Graupner, L. Hammer, K. Heinz, D.M. Zehner, Surf. Sci. 380 (1997) 335.
[6] P.F. Tortorelli, K. Natesan, Mat. Sci. Engng. A 258 (1998) 115.
[7] K. Natesan, Mat. Sci. Engng. A 258 (1998) 126.
[8] J.A. Pfaendtner, R.C. Muthiah, C.T. Liu, C.J. McMahon Jr., Mat. Sci. Engng. A 260 (1999) 1.
[9] S.M. Bruemmer, Mat. Sci. Forum 294–296 (1999) 75.
[10] Zs. Tôkei, J. Bernardini, D.L. Beke, Acta Mat. 47 (1999) 1371.
[11] Y. Mishin, C. Herzig, Mat. Sci. Engng. A 260 (1999) 55.
[12] K. Heinz, L. Hammer, J. Phys.: Condens. Matter 11 (1999) 8377.
[13] R. Hultgren, P.D. Desai, D.T. Hawkins, M. Gleiser, K.K. Kelley, Selected Values of the Thermodynamic Properties of Binary Alloys, American Society of Metals, Metals Park, OH, 1973.
[14] B. Predel, Landolt-Börnstein, New Series, IV/5a, Phase Equilibria, Crystallographic and Thermodynamic Data of Binary Alloys, Springer, Berlin, 1991.
[15] J.M. Sanchez, V. Pierron-Bohnes, F. Mejia-Lira, Phys. Rev. B 51 (1995) 3429.
[16] J.B. Staunton, M.F. Ling, D.D. Johnson, J. Phys.: Condens. Matter 9 (1997) 1281.
[17] M. Polak, L. Rubinovich, Surf. Sci. Rep. 38 (2000) 127.
[18] H. Graupner, L. Hammer, K. Müller, D.M. Zehner, Surf. Sci. 322 (1995) 103.
[19] L. Hammer, H. Graupner, V. Blum, K. Heinz, G.W. Ownby, D.M. Zehner, Surf. Sci. 412/413 (1998) 69.
[20] A.P. Baddorf, S.S. Chandavarkar, Physica B 221 (1996) 141.
[21] D. Voges, E. Taglauer, H. Dosch, J. Peisl, Surf. Sci. 269/270 (1992) 1142.
[22] M. Gemmaz, M. Afyouni, A. Mosser, Surf. Sci. Lett. 227 (1990) L109.
[23] C.P. Wang, F. Jona, N.R. Gleason, D.R. Strongin, P.M. Marcus, Surf. Sci. 298 (1993) 114.
[24] V. Blum, L. Hammer, W. Meier, K. Heinz, 2000, in preparation.
[25] M. Rüsenberg, H. Viefhaus, Ber. Bunsenges. Phys. Chem. 90 (1986) 301.
[26] B. Eltester, C. Uebing, H. Viefhaus, H.J. Grabke, Fresenius J. Anal. Chem. 358 (1997) 196.
[27] M. Kottcke, H. Graupner, D.M. Zehner, L. Hammer, K. Heinz, Phys. Rev. B 54 (1996) R5275.
[28] W. Meier, V. Blum, L. Hammer, K. Heinz, J. Phys.: Condens. Matter, submitted for publication.
[29] K. Heinz, Rep. Progr. Phys. 58 (1995) 637.
[30] H. Wedler, K. Heinz, Vakuum i. Forsch. u. Praxis 7 (1995) 107.
[31] V. Blum, K. Heinz, Comp. Phys. Commun., 2000, in press.
[32] P.J. Rous, J.B. Pendry, D.K. Saldin, K. Heinz, K. Müller, N. Bickel, Phys. Rev. Lett. 57 (1986) 2951.
[33] P.J. Rous, Progr. Surf. Sci. 39 (1992) 3.
[34] R. Döll, M. Kottcke, K. Heinz, Phys. Rev. B 48 (1993) 1973.
[35] U. Löffler, R. Döll, K. Heinz, J.B. Pendry, Surf. Sci. 301 (1994) 346.
[36] K. Heinz, R. Döll, M. Kottcke, Surf. Rev. Lett. 3 (1996) 1651.
[37] M. Kottcke, K. Heinz, Surf. Sci. 376 (1997) 352.
[38] J.B. Pendry, J. Phys. C 13 (1980) 937.
[39] S. Walter, V. Blum, L. Hammer, S. Müller, K. Heinz, M. Giesen, Surf. Sci. 458 (2000) 155.
[40] J. Rundgren, 1999, private communication.
[41] M.P. Thomas, B. Ralph, Surf. Sci. 124 (1983) 151.
[42] Z.Q. Wang, Y.S. Li, F. Jona, P.M. Marcus, Solid State Commun. 61 (1987) 623.
[43] D.E. Gray (Ed.), American Institute of Physics Handbook, McGraw-Hill, New York, 1972.
[44] V. Blum, C. Rath, G.R. Castro, M. Kottcke, L. Hammer, K. Heinz, Surf. Rev. Lett. 3 (1996) 1409.
[45] A. Lawley, R.W. Cahn, J. Phys. Chem. Solids 20 (1961) 204.
[46] L. Hammer, M. Kottcke, M. Taubmann, S. Meyer, C. Rath, K. Heinz, Surf. Sci. 413 (1999) 220.
[47] A. Titov, W. Moritz, Surf. Sci. 123 (1982) 66.
[48] D.L. Adams, H.B. Nielsen, J.N. Andersen, Phys. Scripta T 4 (1983) 22.
[49] F. Lihl, H. Ebel, Arch. Eisenhüttenwesen 32 (1961) 483.
[50] R.J. Corrucini, J.J. Gniewek, Thermal Expans. Tech. Solids at Low Temp., NBS Monogr. 29, Washington, 1961.
[51] V. Pierron-Bohnes, C. Leroux, J.P. Ambroise, A. Menelle, P. Bastie, Phys. Stat. Sol. a 116 (1989) 529.
[52] D. McLean, Grain Boundaries in Metals, Oxford University Press, London, 1957.
[53] T. Schulthess, R. Monnier, S. Crampin, Phys. Rev. B 43 (1994) 18564.
[54] T. Schulthess, E. Wetli, M. Erbudak, Surf. Sci. 320 (1994) L95.
[55] H. Reichert, H. Dosch, T. Hildebrandt, M. Henzler, Verhandl. DPG 35 (VI) (2000) 672.
[56] D. Sondericker, F. Jona, P.M. Marcus, Phys. Rev. B 34 (1986) 6770.
[57] C. Becker, J. Kandler, H. Raaf, R. Linke, T. Pelster, M. Drager, M. Tanemura, K. Wandelt, J. Vac. Sci. Tech. A 16 (1998) 1000.